Viscoelastic analysis of RFDA measurements applied to oxide glasses

Yann Gueguen, Fabrice Célarié, J. Rocherulle, Nourchène Ben Khelil

Viscoelastic analysis of RFDA measurements applied to oxide glasses

Nourchène Ben Khelil[1,2], Yann Gueguen[1], Fabrice Célarié[1], and Jean Rocherullé[2]

[1]Univ Rennes, CNRS, IPR (Institut de Physique de Rennes) - UMR 6251, Rennes, F-35000, France
[2]Univ Rennes, CNRS, ISCR (Institut des Sciences Chimiques de Rennes) - UMR 6226, Rennes, F-35000, France

August 31, 2020

Abstract

The Resonance Frequency and Damping Analysis (RFDA) is now a common experimental technique to measure the elastic moduli of materials *vs.* temperature. Nevertheless, the elastic moduli are calculated assuming that the frequency measured is the natural one, not impacted by any damping. In oxide glasses, a significant damping occurs below the glass transition temperature, and it may impact the frequency measured, the elastic moduli calculated, as well as the estimated glass transition temperature. We show here, using the equations of linear viscoelasticity, how we can know if the frequency measured is significantly lowered by damping, and how we can estimate the natural frequency to calculate the correct elastic moduli, only from the data provided by the RFDA: the frequency measured and the damping.

1 Introduction

The measurement of elastic moduli of glasses is a first and easy measurement to obtain information regarding their structure [1]. Measured *vs.* temperature, it will provide a glass transition temperature, and it allows to track the

relaxation mechanisms of glasses [2, 3, 4]. Among all the methods to measure the elastic moduli of glasses, the Resonance Frequency and Damping Analysis (RFDA) has become very popular, because commercial equipments have been developed, as well as standards, and because it is relatively easy to perform measurements at high temperature. The RFDA method, as endorsed in its name, allows the measurement of a resonance frequency of a material sample and the associated damping. Consequently, the frequency measured is not the natural undamped frequency, but a damped frequency. In a recent study, Wang *et al.* [5] have used various viscoelastic models to investigate RFDA measurements and to determine the viscosity and the non-exponentiality of glass relaxation from the resonance frequency and the damping. It was a pioneer investigation to show that viscoelastic analysis is adapted to the interpretation of the damping. In their investigation, they assume that the measured frequency is very close to the natural, undamped, frequency, and they have investigated glasses where the damping was continuously increasing. Since the damping peak occurs close to the glass transition, where the elastic moduli is supposed to drastically decrease, we could wonder if the frequency drop observed at the glass transition is not only due to the elastic moduli drop but at least partially to the damping, inducing a wrong estimation of the glass transition temperature (T_g) from the slope of the elastic moduli *vs.* temperature. Additionally, from our experience, some glass samples, especially soda-lime silica glasses, exhibit multiple damping peaks *vs.* temperature with clear frequency (f) decrease associated with this damping (i.e.: df/dT show peaks at the same temperatures than damping). As the elastic moduli are calculated assuming that the frequencies measured are not impacted by any damping, this calculation is wrong as soon as the frequencies are too much lowered by damping. The questions we want to solve here are: How do we know if the measured frequency is damped or close to be natural? And how can we recalculate the natural frequency if we measure a damped frequency?

2 Theoretical background

2.1 Natural (undamped) and damped frequencies

For simplicity, to illustrate the problem with simple equations, we use the Euler-Bernoulli beam theory, for a homogenous isotropic sample, in the

framework of pure linear elasticity. For a free beam of length L, cross section S and a second moment of area I_G, the natural frequency f_i of the i^{th} bending mode is given by:

$$f_i = \frac{k_i^2}{2\pi}\sqrt{\frac{I_G}{d\ S\ L^4}}\ \sqrt{E} \tag{1}$$

where E is the Young modulus, and d the density. k_i is the i^{th} solution of the equation $\cos k_i \cosh k_i = 1$. So, $k_1^2 \sim 22.3733$, $k_2^2 \sim 61.6728$, $k_3^2 \sim 120.9032...$ In other words, $f_2/f_1 = 2.7565$ and $f_3/f_1 = 5.4039$. Consequently, the angular frequency ω_i is given by:

$$\omega_i = 2\pi\ f_i = k_i^2\ \beta\ \sqrt{E} \tag{2}$$

where β is a factor that only depends on the sample geometry and the density of the material. More generally, without the assumption of the Euler-Bernoulli beam theory, μ being the shear elastic modulus:

$$\begin{aligned} \omega_i &= \gamma_{E-i}\ \sqrt{E},\ \text{for the bending modes} \\ \omega_i &= \gamma_{\mu-i}\ \sqrt{\mu},\ \text{for the torsion modes} \end{aligned} \tag{3}$$

γ_{E-i} and $\gamma_{\mu-i}$ are factor for the i^{th} mode, that depend on the sample geometry, density, and slightly on the Poisson's ratio.

These frequencies are the natural frequencies, undamped, and as soon as damping occur, the displacement of a given point of the beam, in the bending direction, can be written as (if no over-damping), assuming each point of the beam has a single degree of freedom [6]:

$$u(t) = \sum_i u_{0i}\ \sin\left(\omega_{di}\ t + \varphi_i\right) \exp\left(-\alpha_i\ t\right) \tag{4}$$

ω_{di} is the damped angular frequency ($\omega_{di} < \omega_i$), α_i the exponential decay parameter of the i^{th} mode, φ_i a phase lag. The RFDA method provides the ω_{di} and the α_i, but not ω_i. Consequently if ω_{di} is significantly lower than ω_i, the Young modulus can not be determined using Eq.2 or 3. The questions here are: how do we know that the difference between ω_{di} & ω_i is significant (since ω_i is unknown)? And how can we determine ω_i to find E? And all of this, only with the data provided by the RFDA?

2.2 Viscoelastic model

For simplicity, let us consider first an ideal linear viscoelastic material, with a temperature independent natural frequency. This material has a single relaxation process, temperature dependent. The relaxation time τ of this process decreases when the temperature (T) increases. So relaxing (dissipating) events occur at a typical frequency $1/\tau$, increasing when T increases. The damped frequency will drastically decreases when $1/\tau$ approaches the natural frequency, and the damping increases. Glasses never shows Debye relaxation [**?**], sometimes multi-modal, so that the damped frequency (f_d) will decrease when the natural frequency matches the inverse of the average relaxation time of one of these distributions, producing a damping peak per distribution. Consequently, df_d/dT shows peaks at the same temperature than damping.

In oxide glasses, we usually expect to see, from experience made by Dynamical Mechanical Analysis (DMA), some damping peaks before the glass transition [8, 9], namely the β & γ-relaxation [10] and a large damping when approaching the glass transition, the α-relaxation [10]. The peaks before T_g are basically due to ionic mobilities (alkali, alkali earth): at least one peak per ion and one peak due to a mixed ion effect (γ-relaxation); and are also due to water (β-relaxation) [10]. The peak at T_g is due to the relaxation of the glassy network [10]. Usually the peaks before T_g are convoluted. Because the relaxation time of a glass at T_g is around 100 s, and because samples used in RFDA have resonance frequencies larger than kHz, the peaks are supposed to be shifted to larger temperature, compared to DMA (DMA probing frequency lower than 100 Hz), but are still supposed to be present. From our experience of RFDA, on various oxide glasses, we usually observe, as expected, one broad damping peak before T_g associated sometimes with a small measured frequency (the damped frequency f_d) drop, and a high broad peak starting before T_g, associated with a drastic frequency drop and this is also what is observed by Duang *et al.* [2, 3]. A typical example will be shown later with a soda-lime silica glass. The small frequency drop associated with a low temperature damping peak is also observed in silicon nitride and carbide [11].

The viscoelastic behavior on inorganic glasses can be modelled using a generalised Maxwell model [12], also known as the Wiechert model [13], that is able to describe the dynamic response of inorganic glasses at low and

high frequencies [14, 15], even if its physical meaning can be debated [15]. Let us consider a viscoelastic material using the Wiechert model, to obtain multiple damping peaks, and let us assume that most of the damping is due do viscoelastic dissipation (because it can also be partially due to the wire supporting the sample, the air...). We consider that the Wiechert model has no pure elastic branch, so that its relaxation modulus is (Prony serie):

$$E_R(t) = E \sum_{j=1}^{N} \rho_j \exp\left(-\frac{t}{\tau_j}\right) \tag{5}$$

τ_j are the relaxation times, and $\rho_j \geq 0$ the weight of the j^{th} relaxing process. $\sum_j^N \rho_j = 1$. E_L is the Laplace-Carson transform of $E_R(t)/E$, said "normalised relaxance":

$$E_L(s) = \sum_{j=1}^{N} \rho_j \frac{\tau_j\ s}{1 + \tau_j\ s} \tag{6}$$

s the Laplace variable. The relationship between ω_{di}, α_i and ω_i is given by [16, 17]:

$$\omega_i = \sqrt{\frac{-s_i^2}{E_L(s_i)}} \text{ where } Re(s_i) = -\alpha_i,\ Im(s_i) = \pm\omega_{di} \tag{7}$$

If s_i and $E_L(s_i)$ are known, it is easy to find ω_i. On the other side, when ω_i and $E_L(s_i)$ are known, it is more difficult to find analytical expression for s_i, and thus α_i, ω_{di}. To our knowledge, for $N \geq 4$ no analytical solution has been found. But for $N = 3$, an analytical solution can be found for s_i using computing software, such as Mathematica[1]. We use here this solution for $N = 3$ to calculate s_i and then α_i and ω_{di}.

2.3 Simulation of RFDA measurement

We will investigate how ω_{di} and α_i evolve with temperature for a given Young modulus E and a given evolution of the τ_j. The arbitrary chosen $E(T)$ and $\tau_j(T)$ are plotted on Figure 1. ρ_i are chosen as $\rho_1 = 0.1$, $\rho_2 = 0.2$, $\rho_3 = 0.7$, to qualitatively reproduce the 3 $(\alpha - \beta - \gamma)$ typical damping peaks observed in alkali-oxide glasses [8], but ρ_1 and ρ_2 are chosen 10 times larger than

[1] https://www.wolfram.com/mathematica

their expected values to produce large $\beta - \gamma$ relaxations to make the Figures more readable (increase the hight of the corresponding damping peaks). The Young modulus of glasses under cooling is usually opposite to the volume/enthalpy change. In the supercooled liquid range ($T < T_g$) the volume decreases rapidly under cooling whereas E increases rapidly ($dE/dT = -a$, $a > 0$). When T_g is reach, the volume/enthalpy keeps decreasing but with a lower rate, whereas E increases with a lower rate ($a(T < T_g) < a(T > T_g)$) [14, 18]. $a(T)$ has a temperature dependence very similar to the heat capacity, so that the temperature dependence of E can be predicted using the TNM model [4]. Consequently, under heating at constant heating rate, the Young modulus decreases softly up to T_g and then drops rapidly (this transition is not observed for few glasses, such as fused silica, as an example). The temperature dependence of E used here is chosen to reproduce this typical behavior of inorganic glasses under heating at constant heating rate. The relaxation time τ_j follows arrhenian decays (VFT [19, 20, 21] laws have not be chosen because they diverge, but the arrhenian law is known to be sufficient to described the β and γ relaxations [22]). Again, the parameters for the temperature dependence of the τ_j have be chosen to qualitatively reproduce the $\alpha - \beta - \gamma$ relaxations. For simplicity, we choose the solutions of the Euler-Bernoulli beam theory, with $\beta = 1/k_1^2$ in Eq.2, and at $T = 0K$: $\omega_1 = 1\ rad.s^{-1}$ ($\omega_2 = 2.7565\ rad.s^{-1}$, $\omega_3 = 5.4039\ rad.s^{-1}$), so that the normalised Young modulus at $0K$ is 1.

The corresponding ω_{di} and α_i are calculated using Eq.7 and plotted on Figure 2. As expected, the ω_i show trend similar to E, since $\omega_i \propto \sqrt{E}$, and normalised ω_i are perfectly identical. α_i show roughly 3 peaks at the temperature where $\tau_j \sim 1/\omega_i$ ("roughly" because the peaks are convoluted). The position of the peaks shifts with i, as expected from experiments on glasses: this shift is used to estimate the activation energy of each τ_j [2]. On the other side, the ω_{di} will undergo significant drop every times a damping peak occurs. The drops do not occur at the same temperature for each mode, because each mode "probes" at its own frequency: the equalities $1/\tau_j = \omega_i$ are not reach as the same temperatures. E is also noted E_∞ in rheology, because if its measurement could be made at an infinite frequency, no damping would impact on its measurement, since no relaxation time is ever null: the drops would be virtually shifted to infinite temperature.

What we would have measured for such theoretical material, from the

RFDA, are the ω_{di} and the α_i and nothing else. Consequently, using Eq.2, we would have obtained 3 different "Young moduli", one per mode measured (if 3 modes are measured). We would have known that they are not real Young moduli, since they depend on the mode. This is the first way to know if the frequencies measured are significantly impacted by the damping: if the Young moduli calculated for each mode are identical, the frequencies are closed to the ideal undamped frequencies. Obviously, the best is to have the first mode, and the highest possible mode to have a very large range of frequencies. Now, if we notice that the Young moduli calculated are different from one mode to an other, how can we estimated the "real" Young modulus?

2.4 How to determine the natural frequencies form RFDA measurement?

The undamped frequencies (ω_i) could be calculated from Eq.7, since s_i are known (ω_{di} and α_i are known), but we need to find $E_L(s_i)$ or more specifically the τ_j and the ρ_j. The damping ratio ζ and the Q^{-1} factor are defined as:

$$Q_i^{-1} = 2\,\zeta = \frac{2\alpha_i}{\omega_i} \tag{8}$$

Obviously, since ω_i are not known, we have to assume in this equation that:

$$Q_i^{-1} \sim \frac{2\alpha_i}{\omega_{di}} \tag{9}$$

It is often assumed (but it is not exact [23]), that Q^{-1} is equal to the loss factor:

$$Q_i^{-1} \sim \frac{E''(\omega_i)}{E'(\omega_i)} \tag{10}$$

E'' is the loss modulus, and E' the storage modulus. For our Wiechert model:

$$E'(\omega_i) = E \sum_{j=1}^{N} \rho_j \frac{\tau_j^2 \omega_i^2}{1+\tau_j^2 \omega_i^2}$$
$$E''(\omega_i) = E \sum_{j=1}^{N} \rho_j \frac{\tau_j \omega_i}{1+\tau_j^2 \omega_i^2} \quad (11)$$

Note that E is also noted E_∞ because $E'(\omega \to \infty) = E$. Again, ω_i are not known, so we have to assume:

$$\frac{2\alpha_i}{\omega_{di}} \sim \frac{E''(\omega_{di})}{E'(\omega_{di})} = \frac{\sum_{j=1}^{N} \rho_j \frac{\tau_j \omega_{di}}{1+\tau_j^2 \omega_{di}^2}}{\sum_{j=1}^{N} \rho_j \frac{\tau_j^2 \omega_{di}^2}{1+\tau_j^2 \omega_{di}^2}} \quad (12)$$

With our model, we can test all the approximations made here. $Q_i^{-1} = 2\alpha_i/\omega_i$, approximated $Q_i^{-1} = 2\alpha_i/\omega_{di}$, $E''(\omega_i)/E'(\omega_i)$ and $E''(\omega_{di})/E'(\omega_{di})$ are plotted on Figure 3, for the first and third mode (not the second, for sake of clarity). The results for the other modes are similar. First, the equality supposed in Eq.10 is not perfectly correct, as expected. Then, $E''(\omega_{di})/E'(\omega_{di})$ is a rather good approximation of $2\alpha_i/\omega_{di}$: it slightly overestimates $2\alpha_i/\omega_{di}$ but has identical temperature positions for extremum. Consequently, we can assume that the Eq.12 is quite correct, and so the approximated Q^{-1} (calculated with the damped frequency) can be fitted, as suggested by this equation, by finding the adequate value of τ_j (their temperature dependencies) and ρ_j. We do not need to know E (or ω_i) to fit the approximated Q^{-1}. The $\tau_j(T)$ and ρ_j found can be injected in Eq.7 to find ω_i.

2.5 Maxwell model

In Eq.6, if $N = 1$, we obtain the Maxwell model, that injected in Eq.7 provides the simple and famous relationship:

$$\omega_i = \sqrt{\alpha_i^2 + \omega_{di}^2} \quad (13)$$

And using Eq.9:

$$\omega_i = \omega_{di} \sqrt{\left(\frac{Q_i^{-1}}{2}\right)^2 + 1} \quad (14)$$

We may be tempted to use this simple equation, even when multiple damping peaks occur, because we do not need any data fitting to determine ω_i from α_i & ω_{di}. This equation is applied to our data, using α_1 and ω_{d1} to calculate ω_1. This attempt is plotted on Figure 2 and drastically differs from its expected value, ω_1. Indeed, as indicated by Eq.14, the Maxwell model provides a significant correction of ω_{di} only if Q_i^{-1} is high (1% difference between ω_{di} and ω_i if $Q_i^{-1} > 0.3$), and then rapidly overestimates the correction.

3 Experimental procedure

The experimental measurements have be performed using the impulse excitation technique with the apparatus RFDA HT1050 from IMCE [2]. The experimental procedure, the measurement uncertainties and the method to determine the damping, with this apparatus, have been described by Roebben *et al.* [24]. The sample is supported by thin wires (0.1 mm in diameter) made of PtRh10%, placed at nodes of a given vibration mode, and impacted close to an anti-node of the same vibration mode. The sample is in a furnace, and the acoustic signal is recorded through a microphone, placed outside the furnace (described in [24]) at a top of an alumina rode used as a guide for the acoustic wave. The signal is recorded by the computer and a software interpolates the recorded data through Eq.4 optimising iteratively the parameters u_{0i}, ω_{di}, φ_i and α_i at each temperature. As an output, the software provide the ω_{di} and α_i. Using the resonance frequencies measured, the software also provides the elastic moduli according to ASTM C 1259-94, but we have recalculated the elastic moduli using Finite Element Analysis, with the software Cast3M [3].

4 Results and analysis

We have selected two samples to test our model, with opposite behavior: one where the damping does not induce significant frequency drop (soda-lime silica glass), and one where multiple damping peaks induce multiple frequency drops (phosphate glass).

[2] https://www.imce.eu/

[3] http://www-cast3m.cea.fr/

4.1 Soda-lime silica glass sample

The first sample is a soda-lime silica glass: the window glass Planilux from Saint Gobain. The sample geometry is $75.32 \pm 0.02 \times 20.24 \pm 0.02 \times 2.88 \pm 0.02$ mm^3 heated up at 10 K/min, with a density at room temperature of 2.50 ± 0.01 $g.cm^{-3}$. The supporting PtRh wire were placed at the nodes of the first torsion mode. With this configuration, we succeed to obtain the 5 first resonance frequencies, 3 corresponding to bending, 2 to torsion. From ultrasound velocity measurement, we have [25, 26], at room temperature $E = 71.5 \pm 0.5$ GPa, $\nu = 0.21 \pm 0.01$ and $\mu = 29.5 \pm 0.5$ GPa. Finite Element Analysis have been performed using these values, in order to calculate the resonance frequencies of this sample, using 3D simulation, with all identical cubic elements with 8 nodes, with a total of 486416 nodes, and to calculate the $\gamma_{\mu-i} = f_i/\sqrt{29.5}$ and $\gamma_{E-i} = f_i/\sqrt{71.5}$. The experimental frequencies at room temperature, the γ_{-i} and the corresponding elastic modulus deduced are given in Table 1.

The average elastic moduli found are in the expected range ($E = 72.1 \pm 0.3$ GPa, $\mu = 29.5 \pm 0.2$ GPa), but varie from one mode to another, but these small differences between mode can be just due the sample size uncertainty. The corresponding Poisson's ratio is 0.22 ± 0.01, in the expected range. The measured frequencies *vs.* temperature are plotted on Figure 4.

As we can see on this Figure, the normalised measured frequencies of same deformation modes do not depend on the frequencies. They especially drop exactly the same way, at the same time, above 800 K, showing that this drop is not due to the damping (frequency-dependent) but to a decrease of the elastic moduli. Note that the torsion frequencies do not exactly decrease in the same way as the bending frequencies. This is expected: shear and Young moduli do not have the same temperature dependence, since the Poisson's ratio is itself temperature dependent [14, 18]. The difference between the torsion and bending frequency corresponds to a roughly linear increase of the Poisson's ratio of 0.015 between 300 and 920 K (see inset of Figure 4).

Here, the correction to determine ω from ω_d seems needless, since every frequency provides the same elastic moduli, within experimental uncertainty, at every temperature. Nevertheless, to show that our model does not "over-correct" the experimental data, we will apply our model on these data. The

measured α are shown on Figure 5. Because of the wire position, the damping of the first and third bending mode, as well as the second torsion mode are noisy, because the wires limit the amplitude of these modes. But this configuration is the best one to obtain that much resonance frequencies with significant amplitudes. We assume that the viscoelastic model associated with this glass is a Wiechert model with $N = 4$ cells, and we fit the measured α using Eq.12:

$$\alpha(T) = \frac{\omega_d(T)}{2} \frac{\sum_{j=1}^{N} \rho_j \ \frac{\tau_j(T) \ \omega_d(T)}{1+\tau_j(T)^2 \ \omega_d(T)^2}}{\sum_{j=1}^{N} \rho_j \ \frac{\tau_j(T)^2 \ \omega_d(T)^2}{1+\tau_j^2 \ \omega_d(T)^2}} \tag{15}$$

where, with E_{aj} the activation energy of the relaxation process j:

$$\tau_j(T) = \tau_{0j} \ \exp\left(\frac{E_{aj}}{RT}\right) \tag{16}$$

The α measured for the bending and torsion are fitted with the same parameters, even if they are no supposed to be identical, because the last one involves almost pure shear viscoelastic processes, whereas the other involved also bulk viscoelastic processes. The fitting parameters are given in Table 2. With these fitting parameters, we calculate the relaxance and s_i at any temperature to identify the undamped frequency ω_i from Eq.7, for each mode, and we calculate the corresponding elastic moduli. They are shown on Figure 4. As one can see, the difference between the moduli calculated with damped frequencies and undamped frequencies is very low, as expected. However, one can also see that at $T > 500K$, the damped frequencies show a very small drop associated with the corresponding damping: this is highlighted by the correction made, because we see that only above 500 K the damped and undamped frequencies do not overlap. Our model just corrects this very small effect of damping.

4.2 Phosphate glass

The second sample is a $NaCa(PO_3)_3$ glass. The sample geometry is $35.74 \pm 0.02 \times 13.91 \pm 0.02 \times 4.96 \pm 0.02 \ mm^3$ heated up at 5 K/min, with a density at room temperature of $2.60 \pm 0.01 \ g.cm^{-3}$. The supporting platinum wire were placed at the nodes of the first torsion mode. For this sample we have measured two frequencies corresponding to the first bending and to the first torsion mode (16653 and 23836 Hz respectively at room temperature). All

other frequency modes have too weak signals. The two modes measured are very similar in their temperature dependence, we focus on the torsion mode here. The data are plotted on Figure 6. As we can see, the frequency measured undergoes "oscillations", decreasing every time a damping peak occurs. 9 damping peaks can be distinguished between 475 and $750K$. We will not try to discuss here the physical origin of this peak: This large number of peaks could be assigned hydroxide ions mobilities and their interactions with Na^+ & Ca^{2+}, but they obviously do not correspond to 9 different glass transitions. Even if we do not have the frequencies of the other torsion modes, we clearly know that the frequency measured is a damped frequency. We can not calculate an elastic modulus with it, directly, and we can not define a glass transition from this data. Consequently, we will use our method to calculate the undamped frequency. We assume that the viscoelastic model associated with this glass is a Wiechert model with $N = 9$ cells, and we fit the measured α using Eq.15.

Our best fitting is shown on Figure 6, and the fitting parameters are given in Table 3. Some parameters clearly indicate that the Arrhenius law is not the best to fit the data (some τ_0 do not have any physical sense), but again, the VFT will diverge.

With these fitting parameters, we calculate the relaxance and s at any temperature to identify the undamped frequency ω from Eq.7. As one might expect, the right side of this equation has an imaginary part, but very small. We take the modulus for our calculation. The result is shown on Figure 6. As we can see, all the small drops of the damped frequency have disappeared on the calculated undamped frequency, as expected. At $\sim 685K$ a sharp decrease of the undamped frequency is observed, associated with some noise, due to the noise on the α measured. It is consistent with the Young modulus drop expected at the glass transition temperature, expected to be around $670 - 700K$ for this glass: our model does not eliminate this drop because it is not due to damping. If we try to calculate the undamped frequency using Eq.13-14, the frequency obtained is indistinguishable from the damped frequency, underlying that this simple model is not suitable.

It is sometimes assumed that [27]:

$$\omega_{di} \sim \gamma_{\mu-i} \sqrt{E'(\omega_{di})} \tag{17}$$

From Eq.11, substituting E by μ (E_R by G, E' by G', E'' by G''... terms related to Young moduli by terms related to shear moduli):

$$\mu(T) = \left(\gamma^2 \sum_{j=1}^{9} \rho_j \, \frac{\tau_j(T)^2}{1 + \tau_j(T)^2 \, \omega_d(T)^2} \right)^{-1} \tag{18}$$

All the terms of the right side of this equation are known by direct measurement or fitting. It provides an other equation, different from Eq.7, to determine the elastic moduli. As shown on Figure 7, these two methods (Eq.7 and 18) and are very similar, showing that the approximation of Eq.17 is quite correct.

5 Discussion

Oxide glasses have viscosities larger than 10^{12} Pa.s below T_g, and consequently a relaxation time larger than hundreds of seconds [28]. Centimetric RFDA samples, depending on their densities, and on their elastic moduli, have resonance frequencies larger than kHz. Considering the simple Maxwell model, we could expect $\alpha(T) = (2\tau(T))^{-1}$, and considering Eq.13, if the undamped frequency is around kHz, the measured frequency (damped), should not be even a ppm lower than the undamped frequency, up to T_g. Consequently, we could assume that the RFDA is a suitable method to measure the elastic moduli of oxide glasses up to T_g and a little bit above, because it is not significantly impacted by any damping. Nevertheless, in many oxide glasses low temperature relaxation (β & γ-relaxation) occurs, and it can induce a significant damping, increasing the difference between the undamped and damped frequencies. From our experience on many oxide glasses, the effect of low temperature relaxation can be seen through a small drop of the measured frequency, occurring when the damping associated with this relaxation reaches its maximum. Nevertheless, this drop is not always detectable, depending on the quality of the measurement. A good way to know if the measured frequency is impacted by damping is to compare the evolution of two normalised frequencies, corresponding to the harmonics of a given deformation mode (bending mode, torsion mode...), *vs.* temperature: if they are identical, they are not impacted by damping, if not, they must be corrected. The two examples presented here shown that sometimes this correction is rather needless, sometimes it is a major correction. Unfortunately, measur-

ing multiple frequencies of multiples deformation modes with good intensities and good associated measured damping is not very easy, rather empirical, depending on the sample size and composition, where the sample is impacted and the position chosen for the wires: a given i^{th} mode can be amplified by hitting the sample at its antinode, that would correspond or would be very close to the nodes of other modes and drastically reduce their signals. Experimentally, when, at room temperature, one succeed in having good signal for many modes, frequently, the signal of various modes are lost upon heating. The role of wires and the position where the sample is impacted on the amplitude of the signal, for all the modes where the wires are not at their nodes, or the sample hit at their antinode, is unclear. The sample geometry for the soda-lime-silica glass has be selected after various tests on 21 sample geometries, because it was the one having the larger number of mode with good quality signals. We were not able to produce such a long sample with the phosphate glass.

Note that the fitting parameters in Table 2 do not correspond to the expected equilibrium viscosity of the soda-lime-silica glass ($\eta = \eta_0 \exp(E_a/(RT))$, with $\eta_0 = 2.91 \times 10^{-24}$ Pa.s and $E_a = 571$ kJ/mol [26]), but this is not unexpected. The damping peaks below T_g correspond to, by definition, processes that are not under equilibrium, and the damping peak(s) well above T_g (α relaxation), the major contribution to the viscosity (because its ρ_j is larger), to processes under equilibrium. But this latter can not be properly measured, since the RFDA signal becomes too weak when it occurs (on Figure 5, we just see the beginning of the α peak). Consequently, a viscosity calculated from the fitting of the damping can not be exactly an equilibrium viscosity, and can not be properly calculated since its major contribution is missing. Wang *et al.* [5] succeed in determining the viscosity of their glasses from the damping, but they observe a single large damping peak. It seems that when β & γ-relaxations occur, the viscosity can not be determined anymore from the damping. What is more unexpected is the sharp decrease of the elastic moduli occurring at $T > 850$ K, whereas ultrasonic measurement at 300 kHz, made by Rouxel and Sangleboeuf [29] indicate a sharp decrease at $T \sim 820$ K. Below T_g there is a good agreement between our measurements and these ones, but the sharp elastic moduli decrease due to the glass transition occurs later when measured by RFDA. If our measurement were significantly impacted by damping, we would expect the opposite, since our frequencies are much lower.

We could wonder why for the soda-lime-silica glass the damping peak are convoluted ($N = 4$ in the Wiechert model, but only two visible peaks on Figure 5), whereas the damping peaks of the $NaCa(PO_3)_3$ glass are nicely deconvoluted ($N = 9$ for 9 peaks). Two relaxation processes with different τ_{0j} & E_{aj} (Eq.16) will produce convoluted peaks when they will have similar relaxation time in the temperature range investigated and if this relaxation time is close to the inverse of the natural angular frequency of the sample. So, it is not unexpected to observe situations where peaks are convoluted and other where they are not: for a given glass composition, with RFDA, it will only depends on the sample geometry.

The correction proposed here is based on linear viscoelasticity. We propose to fit the damping measured using a viscoelastic model, the Wiechert model, taking advantage of the fact that, roughly, the damping does not depend on the undamped frequency that is unknown. To our opinion, the chosen model does not need to capture all the detail of the glass relaxation, as soon as it is able to reproduce the damping peaks. As an exemple, below T_g, the glasses are out of equilibrium: their elastic moduli and relaxation times are heating-rate dependent [4]. This is not something taken into account here. All the results presented in this work are thermal history-dependent. But what we want to emphasize here is that the method to eliminate the effect of damping does not need to capture this dependence to properly operate. In return we can not expect to extract physically sounded parameters from the fitting used in the method: we will have to use different fitting parameters for each heating/cooling rate. All we need to apply our method is a viscoelastic model that reproduces the damping at a given heating or cooling rate, even if it does not capture all the physics behind. In other words, all the fitting parameters found here must only be seen as fitting parameters and nothing else. Additionally, if our investigation shows that the measured frequencies do not always allow to determine an elastic moduli, it also shows that it allows to determine the storage moduli at the damped frequencies (Eq.17). Consequently, the RFDA is also a method to determine the loss and storage moduli at relatively high frequencies, compared to DMA, and is a complementary method to DMA.

It must be noticed that when the wire are placed at the node of a given deformation mode, the damping of the other modes are increased [24]. With the configuration we have chosen, where the wire are at the nodes of first torsion mode, it seems that the damping of the first bending mode is not impacted, this is the reason why we have chosen this configuration. We

could expect that, if we fit the damping of the first bending mode with a Wiechert model, this model will be able to predict the damping of all other bending mode. But because of the effect of the wires, this fitting will be quantitatively unsuccessful. However, we can expect a qualitative fitting: a correct prediction of the temperature of the damping peaks. But, again, it is rather difficult to obtain good signals for many modes.

6 Conclusion

Most of oxide glasses exhibit relaxation processes below the glass transition range (β & γ-relaxations). During RFDA measurements, these processes induce a significant damping and this damping can shift the measured frequency to a value significantly lower than the natural frequency of the glass sample, inducing a wrong estimation of the elastic moduli. Using the other frequencies of the same deformation mode than the first one measured, we can control if the frequencies measured are impacted by any damping: if they are not, their normalised evolutions *vs.* temperature overlap, and the elastic moduli can be deduced from these frequencies. If they are impacted by damping, larger frequencies would show drops at larger temperature. Nevertheless, if they are not superimposed, or if the other frequencies are not correctly measured, one can not determine the elastic moduli. We use here the equations of linear viscoelasticity to show how we can determine the elastic moduli using the frequencies measured and the damping. Two equations are used, a first one using the correspondance principle (the Laplace-Carson transform, Eq.7), and a second one assuming that the moduli calculated with the measured frequency is the storage moduli (Eq.18). These two equations provides similar results, removing all apparent elastic moduli drops due to damping, letting the expected "real" drop occurring at T_g. For both equations, we need to fit the damping using a rheological model of linear viscoelasticity, with temperature dependent relaxation times. It seems that the model does not need to capture the complexity of the glass relaxation, but in return does not provides any physically sounded parameters. The one shown here is the Wiechert model, but there is no reason why it would not work with other linear viscoelastic models. To our opinion, for most oxide glasses, this correction is minor (as exemplified with the soda-lime-silica glass), but for some samples, as the phosphate glass investigated here, the correction made on calculated elastic moduli is larger than 14%. Nevertheless, it must

be underlined that the relaxation time of oxide glass around T_g being close to hundreds of seconds, it is not expected to observe any significant damping around T_g when the natural frequency is larger than kHz, but from our experience, most of them show significant damping. This is the reason why we must always pay attention to the frequency measured and ensure that it is not significantly impacted by the damping.

References

[1] J. D. Musgraves, J. Hu, L. E. Calvez (Eds.), Springer handbook of glass, Springer, 2019. Part A, Chapter 7.

[2] R. Duan, G. Roebben, O. V. der Biest, K. Liang, S. Gu, Microstructure research of glasses by impulse excitation technique (IET), Journal of Non-Crystalline Solids 281 (2001) 213 – 220.

[3] R.-G. Duan, G. Roebben, O. V. der Biest, Glass microstructure evaluations using high temperature mechanical spectroscopy measurements, Journal of Non-Crystalline Solids 316 (2003) 138 – 145.

[4] W. Liu, H. Ruan, L. Zhang, Revealing structural relaxation of optical glass through the temperature dependence of young's modulus, Journal of the American Ceramic Society 97 (2014) 3475–3482.

[5] J. Wang, H. Ruan, X. Wang, J. Wan, Investigating relaxation of glassy materials based on natural vibration of beam: A comparative study of borosilicate and chalcogenide glasses, Journal of Non-Crystalline Solids 500 (2018) 181 – 190.

[6] E. Gregorova, W. Pabst, P. Dibliková, V. Nečina, Temperature dependence of damping in silica refractories measured via the impulse excitation technique, Ceramics International 44 (2018) 8363 – 8373.

[7] R. Böhmer, K. Ngai, C. Angell, D. Plazek, Nonexponential relaxations in strong and fragile glass formers, Journal of Chemical Physics 99 (1993) 4201–4209.

[8] W. A. Zdaniewski, G. E. Rindone, D. E. Day, The internal friction of glasses, Journal of Materials Science 14 (1979) 763–775.

[9] B. Roling, Mechanical loss spectroscopy on inorganic glasses and glass ceramics, Current Opinion in Solid State and Materials Science 5 (2001) 203–210.

[10] J. Deubener, H. Bornhöft, S. Reinsch, R. Müller, J. Lumeau, L. Glebova, L. Glebov, Viscosity, relaxation and elastic properties of photo-thermo-refractive glass, Journal of Non-Crystalline Solids 355 (2009) 126 – 131.

[11] G. Roebben, R.-G. Duan, D. Sciti, O. V. der Biest, Assessment of the high temperature elastic and damping properties of silicon nitrides and carbides with the impulse excitation technique, Journal of the European Ceramic Society 22 (2002) 2501 – 2509.

[12] L. Duffrène, R. Gy, H. Burlet, R. Piques, Viscoelastic behavior of a soda-lime-silica glass: inadequacy of the KWW function, Journal of Non-Crystalline Solids 215 (1997) 208–217.

[13] E. Wiechert, Gesetze der elastischen nachwirkung für constante temperatur, Annalen der Physik 286 (1893) 546–570.

[14] L. Duffrène, R. Gy, J. E. Masnik, J. Kieffer, J. D. Bass, Temperature dependence of the high-frequency viscoelastic behavior of a soda-lime-silica glass, Journal of the American Ceramic Society 81 (1998) 1278–1284.

[15] L. Duffrène, R. Gy, H. Burlet, R. Piques, A. Faivre, A. Sekkat, J. Perez, Generalized maxwell model for the viscoelastic behavior of a soda-lime-silica glass under low frequency shear loading, Rheologica acta 36 (1997) 173–186.

[16] N. W. Tschoegl, The phenomenological theory of linear viscoelastic behavior: an introduction., Springer Science & Business Media, 2012.

[17] P. Djoharian, Shape and Material Design in Physical Modeling Sound Synthesis, in: ICMC 2000 - International Computer Music Conference, Berlin, Germany, 2000, p. n/c. 8 pages.

[18] T. Rouxel, Elastic properties and short to medium range order in glasses., Journal of the American Ceramic Society 90 (2007) 3019–3039.

[19] H. Vogel, Das temperature-abhängigketsgesetz der viskosität von flüssigkeiten, Phys. Z. 22 (1921) 645–6.

[20] G. S. Fulcher, Analysis of recent measurements of the viscosity of glasses, Journal of the American Ceramic Society 8 (1925) 339–355.

[21] G. Tammann, W. Hesse, Zeitschrift fur anorganische und allgemeine Chemie 156 (1926) 245–257.

[22] J. Perez, P. Gobin, Phénomènes de relaxation et frottement intérieur dans les solides vitreux, Revue de Physique Appliquée 12 (1977) 819–836.

[23] M. Carfagni, E. Lenzi, M. Pierini, The loss factor as a measure of mechanical damping, In Proceedings-spie the international society for optical engineering. SPIE INTERNATIONAL SOCIETY FOR OPTICAL Vol. 1 (1998) 580–284.

[24] G. Roebben, B. Bollen, A. Brebels, J. Van Humbeeck, O. Van der Biest, Impulse excitation apparatus to measure resonant frequencies, elastic moduli, and internal friction at room and high temperature, Review of Scientific Instruments 68 (1997) 4511–4515.

[25] C. Bernard, Indentation and rheology of inorganic glasses from 20 to 700 °C, Thesis, Université Rennes 1, 2006.

[26] C. Bernard, V. Keryvin, J.-C. Sangleboeuf, T. Rouxel, Indentation creep of window glass around glass transition, Mechanics of Materials 42 (2010) 196 – 206.

[27] I. Popov, T. P. Chang, Y. Rossikhin, M. Shitikova, Experimental investigation of fly ash and water content on the internal friction of concrete, in: Second International Conference on Mechanics, Materials and Structural Engineering (ICMMSE 2017). Atlantis Press., 2017.

[28] C. Angell, Relaxation in liquids, polymers and plastic crystals strong/fragile patterns and problems, Journal of Non-Crystalline Solids 131-133 (1991) 13–31.

[29] T. Rouxel, J.-C. Sangleboeuf, The brittle to ductile transition in a soda-lime-silica glass, Journal of Non-Crystalline Solids 271 (2000) 224 – 235.

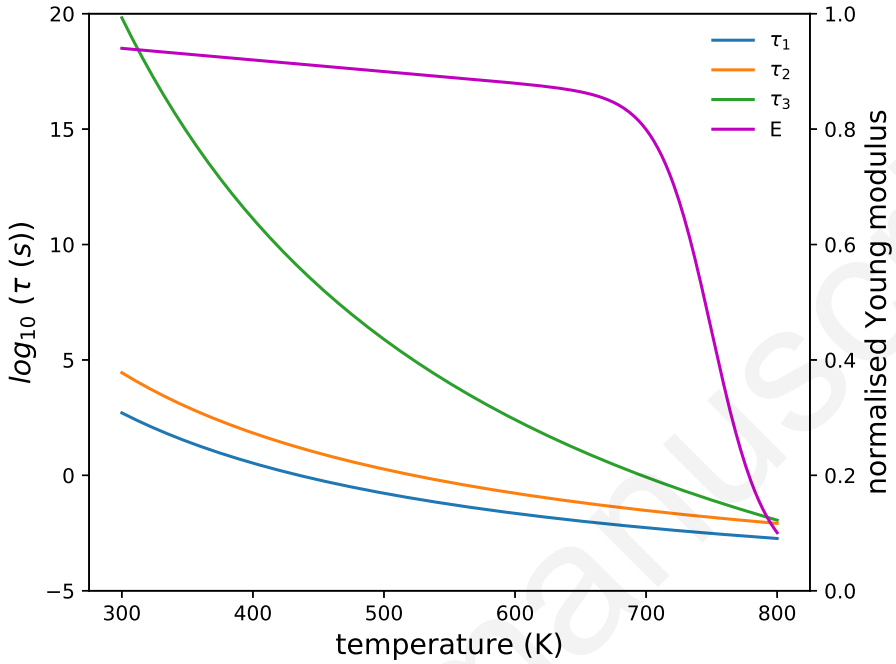

Figure 1: Young modulus (normalised by its value at $0K$, on the right) and relaxation times (τ_j) used for the simulation (on the left).

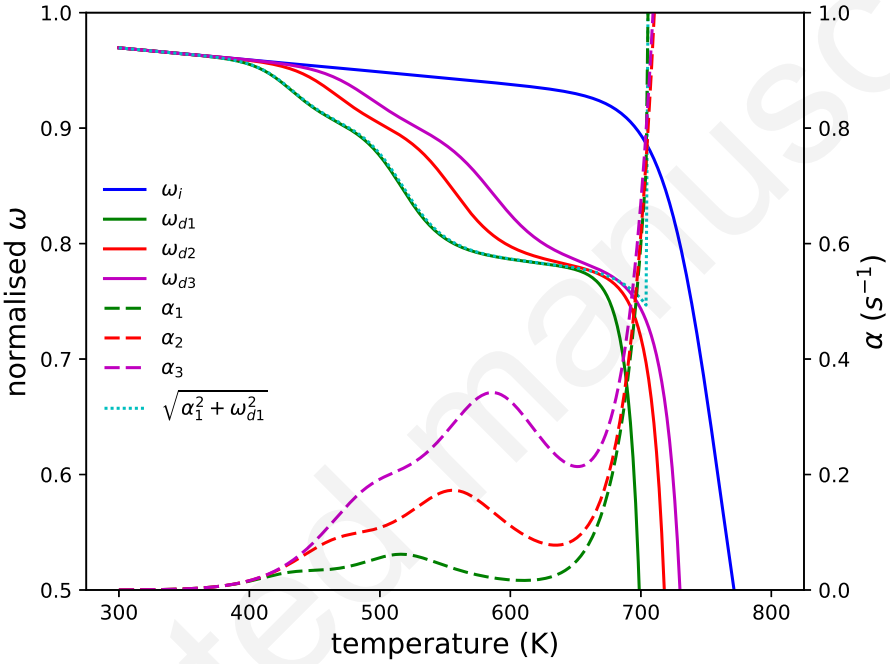

Figure 2: Left axis: Normalised natural (undamped) frequencies ω_i (all superimposed) and damped frequencies ω_{di} of the i^{th} bending mode (decreasing curves). They are normalised by their values at $0K$. Each bending mode gives the same normalised natural frequency. Right axis, dashed: corresponding α_i (increasing curves).

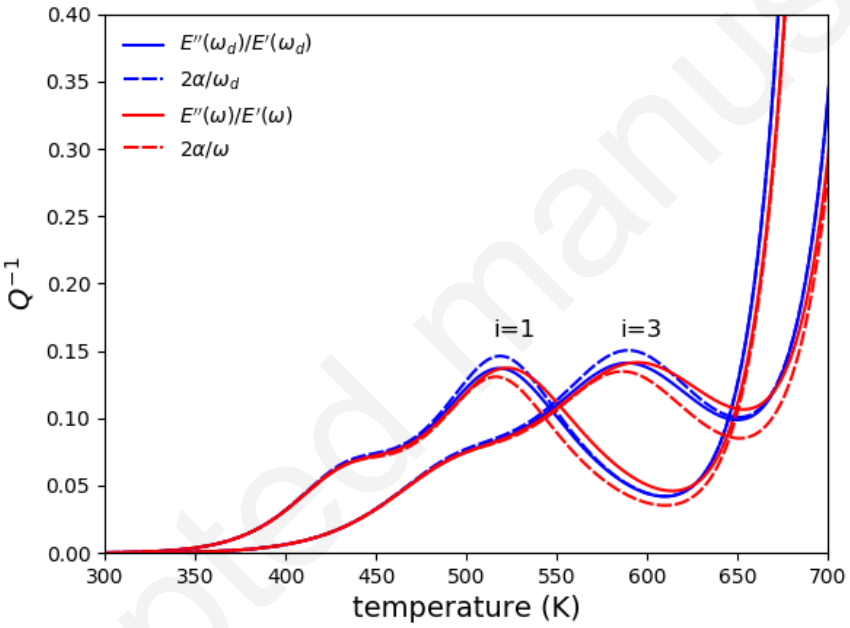

Figure 3: Comparison between "exact" $Q_i^{-1} = 2\alpha_i/\omega_i$, approximated $Q_i^{-1} = 2\alpha_i/\omega_{di}$, $E''(\omega_i)/E'(\omega_i)$ and $E''(\omega_{di})/E'(\omega_{di})$, for $i = 1$ & 3.

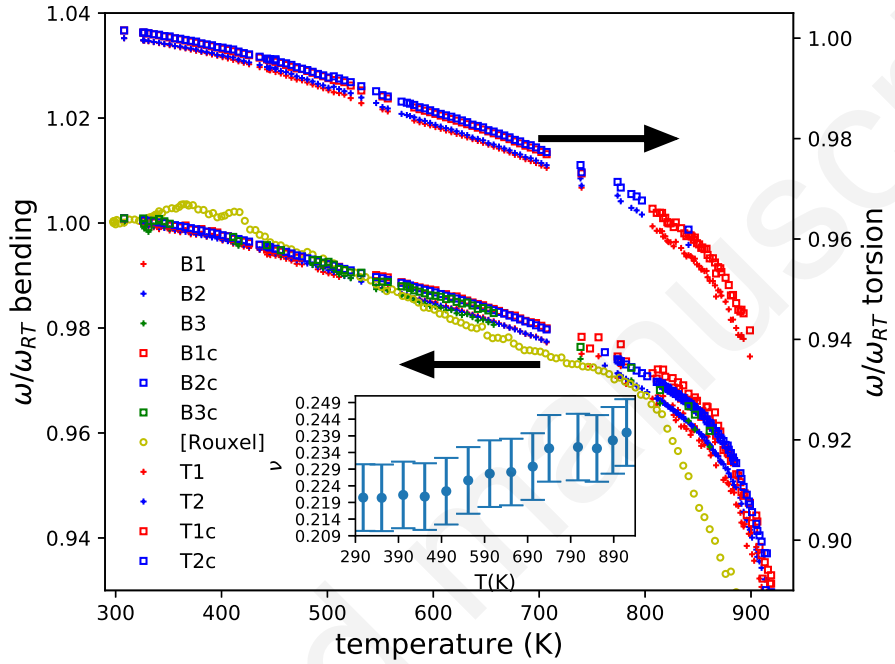

Figure 4: Data for the Planilux sample. Normalised measured pulsations (by the pulsations at room temperature ω_{RT}) vs temperature (equivalent to normalised measured frequencies: the frequencies are normalised by the values in Table 1): Bi: i^{th} bending mode -bottom-, Ti: i^{th} torsion mode -top-, and normalised calculated undamped frequencies: Bic: i^{th} bending mode, Tic: i^{th} torsion mode. Inset: corresponding evolution of the Poisson's ratio, calculated form the first bending and torsion modes. The square root of the normalised Young Modulus measured by Rouxel and Sangleboeuf is also given [29]: ultrasonic measurements, using the long beam mode configuration, at 300 kHZ, under nitrogen atmosphere. For this measurement: $E(300K) = 72 \pm 1\ GPa$.

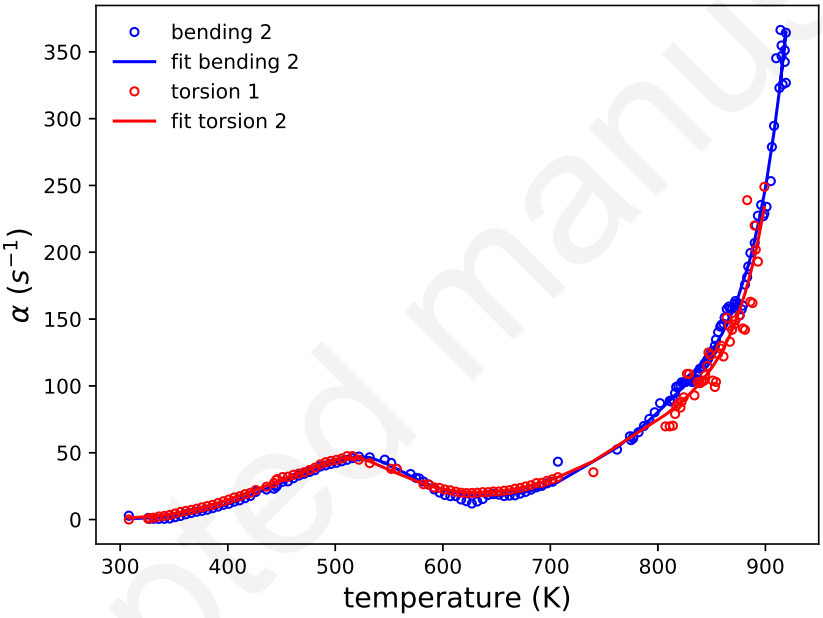

Figure 5: α measured for the Planilux sample, for the second bending mode and the first torsion mode.

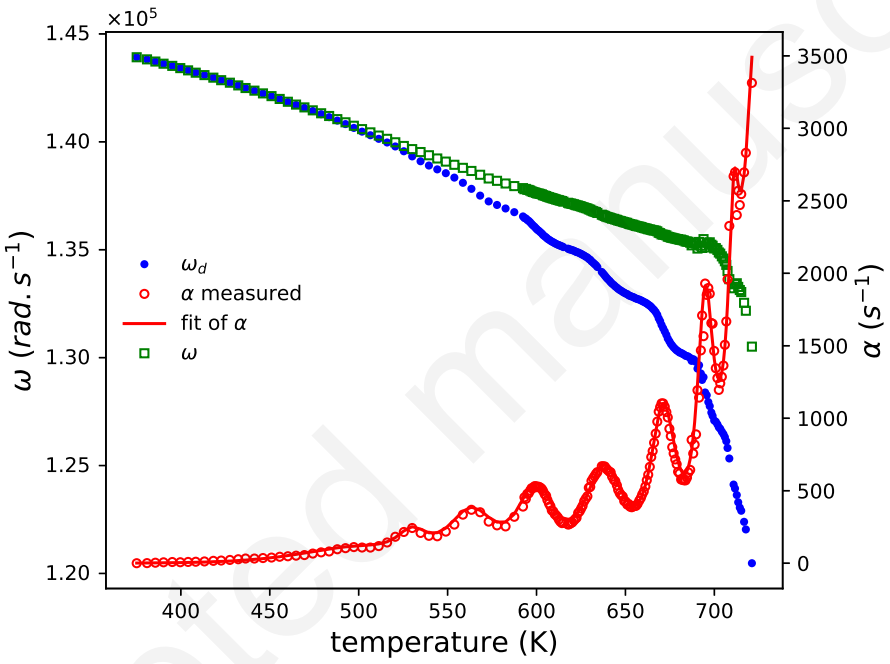

Figure 6: Measured angular frequency (named ω_d), calculated undamped angular frequency (ω) and corresponding α, measured and fitted, for the first torsion mode of the $NaCa(PO_3)_3$ sample.

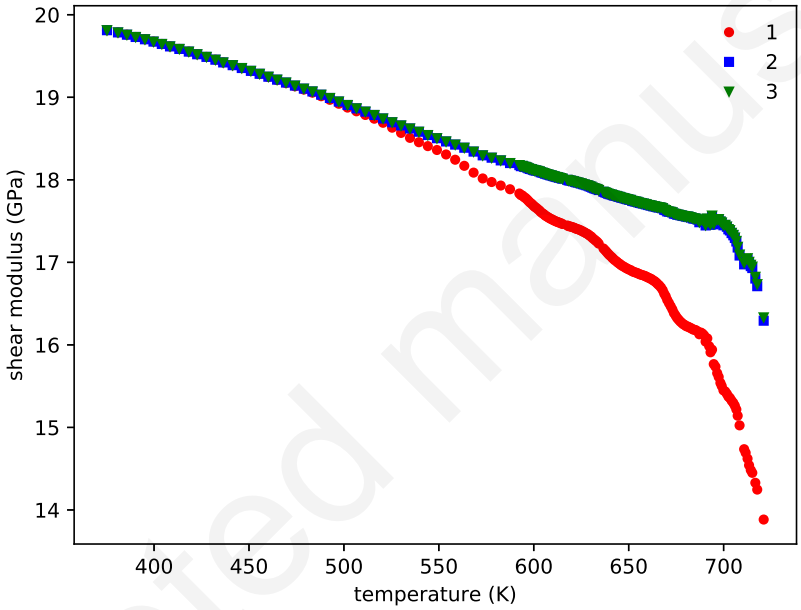

Figure 7: Calculated shear elastic modulus μ, directly given by the RFDA software (1), using $\omega = \gamma\sqrt{\mu}$, where ω is the calculated undamped angular frequency (2) and assuming $\omega_d = \gamma\sqrt{G'(\omega_d)}$ (3). G' being the equivalent of E' in shear.

Table 1: 5 first experimental and FEA frequencies for the Planilux sample at room temperature, γ_i (= $\gamma_{\mu-i}$ for torsion, γ_{E-i} for bending) calculated from FEA, and deduced elastic moduli E from experimental frequencies of bending, μ from torsion.

mode	i	f exp. ($\pm 1\ Hz$)	f FEA (Hz)	γ_{-i} $(s.\sqrt{GPa})^{-1}$	E or μ ($\pm 0.1\ GPa$)
bending	1	2799	2795	330	71.9
torsion	1	6243	6220	1153	29.3
bending	2	7681	7653	905	72.2
torsion	2	12907	12830	2378	29.6
bending	3	14921	14839	1755	72.4

Table 2: Fitting parameters for α of the Planilux sample.

j	$E_a\ (kJ/mol)$	$-log_{10}(\tau_0)$	ρ
1	58	10.4	0.003
2	34	8.5	0.002
3	68	8.8	0.008
4	203	14.3	0.987

Table 3: Fitting parameters for α of the $NaCa(PO_3)_3$ sample.

j	$E_a\ (kJ/mol)$	$-log_{10}(\tau_0\ (s))$	ρ
1	66	12	0.003
2	330	38	0.004
3	235	27	0.010
4	330	34	0.014
5	343	33	0.018
6	586	51	0.028
7	1047	84	0.041
8	1737	133	0.031
9	323	27	0.851